Mode-III Stress Intensity Factors of a Three-Phase Composite with an Eccentric Circular Inclusion

C.K. Chao[1] and A. Wikarta[1]

Abstract: An analytical solution to a three-phase composite with an eccentric circular inclusion under a remote uniform shear load is given in this work. Mode-III stress intensity factors for an arbitrarily oriented crack embedded in an infinite matrix or a core inclusion are provided in this paper. Based on the method of analytical continuation in conjunction with the alternating technique, the solution for a screw dislocation located either in the core inclusion or in the infinite matrix is first derived in a series form. The integral equations with logarithmic singular kernels for a line crack are established by using the screw dislocation solutions as the Green's function together with the principle superposition. The stress intensity factors, which can properly reflect the interaction between a crack and a non-uniformly coated circular inclusion, are then obtained numerically in terms of the values of the dislocation density functions of the integral equations. The effects of material property combinations and geometric parameters on the normalized mode-III stress intensity factors are discussed in detail and shown in graphic form.

Keywords: an eccentrically coated circular inclusion, arbitrarily oriented crack, alternating technique, mode-III stress intensity factors.

1 Introduction

The interaction between cracks and inhomogeneities has received appreciable attention in evaluating the degree of failure of composite structures. In order to solve the crack problem, the fundamental solution for a point dislocation is widely used to treat as a Green's function. By placing the dislocation density function along the prospective site of crack, the singular integral equations are then formulated. Applying the Kernel with Cauchy type singularity, the interaction of cracks with inhomogeneities has been solved by several researchers. [Atkinson (1972); Erdogan, Gupta, and Ratwani (1974)] obtained the solution for a crack outside circular inclusion, and [Erdogan and Gupta (1975)] presented the problems of a crack

---

[1] NTUST, Taipei, Taiwan, ROC.

inside circular inclusion. An alternative method for solving crack problems by formulating the kernel in terms of logarithmic singular has also been developed by many researchers. [Chen and Cheung (1990)] gave an elementary solution for the crack problem in elastic half plane. The thermoelastic crack problems were solved by [Chao and Shen (1995); Chao and Lee (1996)] for crack in bonded dissimilar media interacted with a circular elastic inclusion. [Chen and Chen (1997)] evaluated the curved crack problem in an infinite plate containing the elastic inclusion. Recently, [Wang and Zhong (2003)] proposed a model of a non-uniformly coated circular inclusion interacting with screw dislocation in an infinite matrix under anti-plane deformations. This problem was solved by using conformal mapping technique. Based on the same technique, [Chen (2011)] studied the edge dislocation interacting with a non-uniformly coated circular inclusion in plane elasticity. Meanwhile, [Shen, Chen, and Chen (2006)] investigated the interaction of a piezo-electric screw dislocation with a non-uniformly coated circular inclusion by using alternating technique.

In this paper, anti-plane interaction between an eccentrically coated circular inclusion and a crack located either in an infinite matrix or in a core inclusion is solved by applying the solution of dislocation as a Green's function. The proposed method is based on the technique of analytical continuation that is alternately applied across two different interfaces. To analyze the interaction between a crack and a non-uniformly coated circular inclusion, the existing solutions for dislocation functions are used to formulate the logarithmic singular integral equations for a line crack, and mode-III stress intensity factors are obtained numerically. The layout of the present paper is as follows. The problem statement and homogeneous solution for anti-plane elasticity is introduced in Section 2. The series form solutions for the complex potentials function are given in Section 3. The integral equations with logarithmic singular kernels for a line crack are established in Section 4. Some numerical examples are solved in Section 5. Finally, Section 6 concludes the article.

2 Model

Consider a cross section of an eccentrically coated circular inclusion in an infinite matrix subjected to a remote uniform shear load as shown in Figure 1. A line crack is assumed to be located either in an infinite matrix or in core inclusion. Let S_1 denote the infinite matrix, S_2 denote the coating layer, and S_3 denote the core inclusion, respectively. The boundaries of coating layer are two circles Γ_1 and Γ_2 which are assumed to be perfect, i.e. both tractions and displacements are continuous across the two interfaces. The origin of the Cartesian coordinate system is chosen to be at the center of the outer circle Γ_1 of unit radius. The center of the inner circle Γ_2 of radius $r = (x_2 - x_1)/2$ lies on the x-axis. The two centers of the
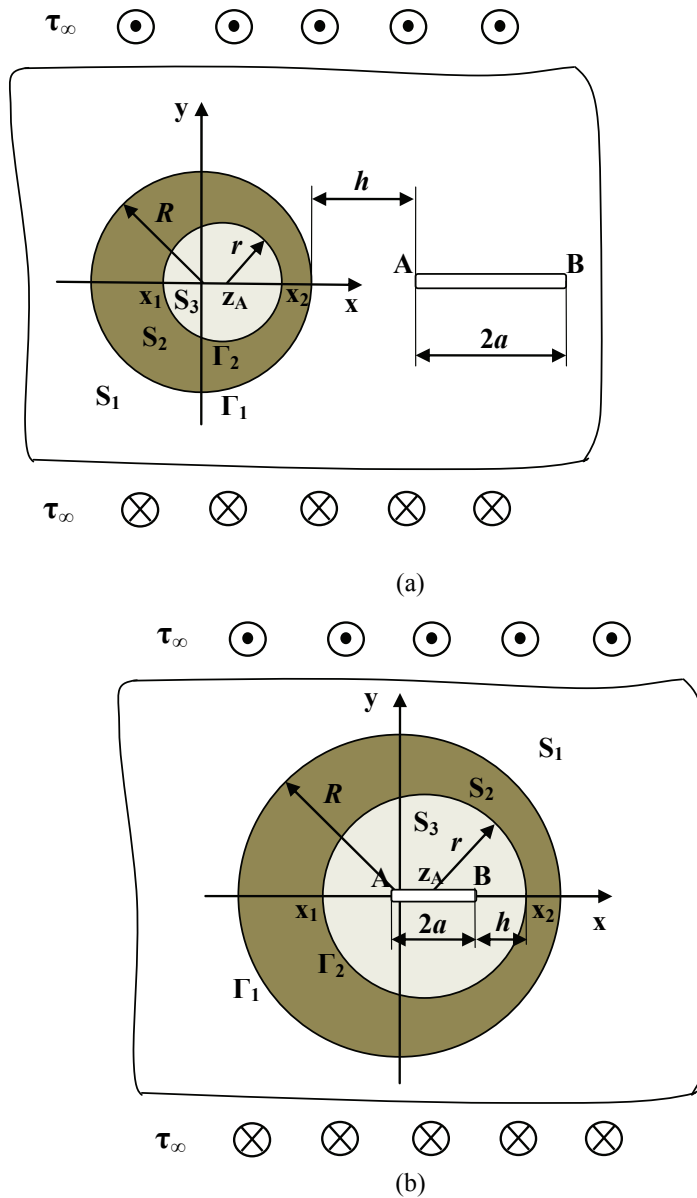
Figure 1: A non-uniformly coated circular inclusion with (a) a crack located in infinite matrix and (b) a crack located in core inclusion subjected to a remote uniform shear load.

two circles Γ_1 and Γ_2 are set apart by the distance $\Delta = (x_2 + x_1)/2$. Let the infinite matrix (or core inclusion) contain a line crack with length 2*a* which is located along *x*-axis with distance *h* away from outer (or inner) circle interface. In addition, a remote uniform shear load is assumed to be directed at an angle 90˚ from *x*-axis. Based on the complex variable theory for a two-dimensional anti-plane elasticity, the resultant force *P* and displacement ω can be written in terms of a single complex potential $\theta(z)$ as follows:

$$P = \int (\tau_{xz}dy - \tau_{yz}dx) = -\frac{Im}{2}[\theta(z)] \tag{1}$$

$$\omega = \frac{1}{2\mu}Re[\theta(z)] \tag{2}$$

where Re and Im denote the real part and imaginary part of the bracketed expression, respectively. The quantities τ_{xz} and τ_{yz} are the components of shear stresses in x and y direction, respectively. (') is designated as the derivative with respect to the associated argument and μ stands for the shear modulus. Once the anti-plane problem is solved, the complex potential $\theta(z)$ is determined.

The complex potential for an infinite homogeneous medium subjected to a remote uniform shear load τ_∞ directed at an angle 90˚ from *x*-axis is given by the simple expression

$$\theta_0(z) = -i\tau_\infty z \tag{3}$$

In order to solve crack problems, the complex potentials for an infinite homogeneous medium subjected to a screw dislocation with Burgers vector b_0 located at $z = z_t$ are introduced as

$$\theta_0(z) = \frac{b_0}{2\pi i}\log(z - z_t) \tag{4}$$
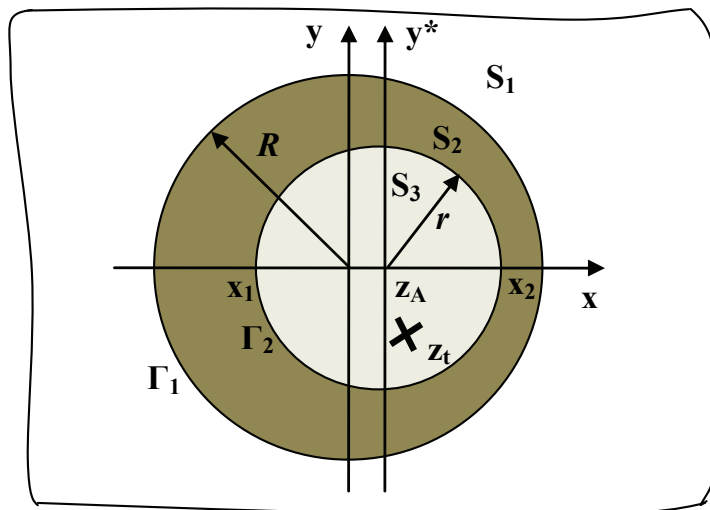
3   Solution

In this section, we will derive the complex potential for a non-uniformly coated circular inclusion subjected to a screw dislocation in an infinite matrix or in core inclusion as shown in Fig. 2.

3.1   *Screw dislocation in infinite matrix*

First, we consider a screw dislocation located in an infinite matrix. In order to satisfy the continuity conditions of each interface, the complex potential functions
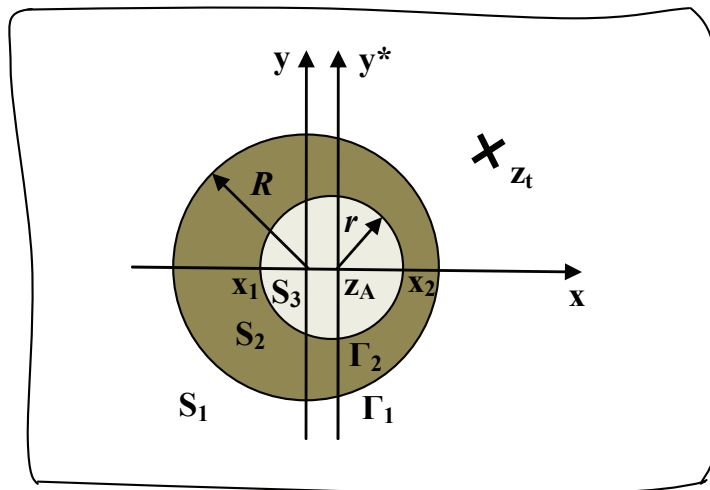
(a)

(b)

Figure 2: A non-uniformly coated circular inclusion with (a) a screw dislocation located in infinite matrix and (b) a screw dislocation located in core inclusion.

of each medium can be assumed as.

$$
\theta(z) = \begin{cases}
\sum\limits_{n=1}^{\infty} \theta_{an}(z) & z \in S_3 \\
\sum\limits_{n=1}^{\infty} \theta_n(z) + \sum\limits_{n=1}^{\infty} \theta_{bn}(z) & z \in S_2 \\
\theta_0(z) + \theta_{c0}(z) + \sum\limits_{n=1}^{\infty} \theta_{cn}(z) & z \in S_1
\end{cases}
\tag{5}
$$

In order to determine the complex functions $\theta(z)$ for a non-uniformly coated circular inclusion subjected to a screw dislocation as shown in Fig. 2, the alternating technique is applied by the following procedure.

Step 1: Analytical continuation across the interface Γ_1

First, we regard regions S_2 and S_3 composed of the same material μ_2 and region S_1 of material μ_1. If $\theta_0(z)$ represents a complex function in an infinite homogeneous medium, $\theta_{c0}(z)$ analytical in $z \geq R$ and $\theta_1(z)$ analytical in $z \leq R$ are introduced to satisfy the continuity conditions of the displacement and the resultant force across Γ_1, so that

$$
\mu_2 \left\{ \theta_0(t) + \overline{\theta_0(t)} + \theta_{c0}(t) + \overline{\theta_{c0}(t)} \right\} = \mu_1 \left\{ \theta_1(t) + \overline{\theta_1(t)} \right\}
\tag{6}
$$

$$
\theta_0(t) - \overline{\theta_0(t)} + \theta_{c0}(t) - \overline{\theta_{c0}(t)} = \theta_1(t) - \overline{\theta_1(t)}
\tag{7}
$$

By the standard analytical continuation theorem one obtains

$$
\theta_{c0}(z) = V_{21} \overline{\theta_0} \left(\frac{R^2}{z} \right) \quad z \geq R
\tag{8}
$$

$$
\theta_1(z) = U_{12} \theta_0(z) \quad z \leq R
\tag{9}
$$

where $V_{jk} = \frac{\mu_k - \mu_j}{(\mu_j + \mu_k)} U_{jk} = \frac{2\mu_k}{(\mu_j + \mu_k)}$.

Since this result is based on the assumption that region S_3 is made up of material μ_2, $\theta_1(z)$ cannot satisfy the continuity conditions at the interface Γ_2, which lies between material μ_2 and μ_3.

Step 2: Analytical continuation across the interface Γ_2

We next assume that region S_3 is composed of material μ_3 and regions S_1 and S_2 are regarded as made up of the same material μ_2. Additional terms $\theta_{a1}(z)$ analytical in $z \leq r$ and $\theta_{b1}(z)$ analytical in $z \geq r$ are introduced to satisfy the continuity conditions of the displacement and the resultant force across the interface Γ_2, so that

$$
\mu_3 \left\{ \theta_{a1}^*(t^*) + \overline{\theta_{a1}^*(t^*)} \right\} = \mu_2 \left\{ \theta_1^*(t^*) + \overline{\theta_1^*(t^*)} + \theta_{b1}^*(t^*) + \overline{\theta_{b1}^*(t^*)} \right\}
\tag{10}
$$

$$\theta_{a1}^*(t^*) - \overline{\theta_{a1}^*(t^*)} = \theta_1^*(t^*) - \overline{\theta_1^*(t^*)} + \theta_{b1}^*(t^*) - \overline{\theta_{b1}^*(t^*)} \tag{11}$$

Here, '*' denotes the field in $x * y*$ system. By the standard analytical continuation theorem one can obtain

$$\theta_{a1}^*(z^*) = U_{23}\theta_1^*(z^*) \quad z \le r \tag{12}$$

$$\theta_{b1}^*(z^*) = V_{32}\overline{\theta_1^*}\left(\frac{r^2}{z^*}\right) \quad z \ge r \tag{13}$$

With a coordinate translation $z^* = z - z_A$ (see Fig. 2), it is easy to show that the complex potential in the xy coordinate system is related to the function in the $x * y*$ coordinate system by

$$\theta^*(z^*) = \theta(z) \tag{14}$$

$$\overline{\theta^*}\left(\frac{r^2}{z^*}\right) = \overline{\theta}\left(\frac{r^2}{z - z_A} + \overline{z_A}\right) \tag{15}$$

Substituting of Eqs. (14) and (15) into Eqs. (12) and (13) yields

$$\theta_{a1}(z) = U_{23}\theta_1(z) \tag{16}$$

$$\theta_{b1}(z) = V_{32}\overline{\theta_1}\left(\frac{r^2}{z - z_A} + \overline{z_A}\right) \tag{17}$$

Since this result is based on the assumption that region S_1 is made up of material μ_2, $\theta_{b1}(z)$ cannot satisfy the continuity conditions at the interface Γ_1, which lies between material μ_2 and μ_1.

Step 3: Analytical continuation across the interface Γ_1

We again assume regions S_2 and S_3 composed of the same material μ_2 and region S_1 of material μ_1. Additional terms $\theta_2(z)$ holomorphic in $z \le R$ and $\theta_{c1}(z)$ holomorphic in $z \ge R$ are introduced to satisfy the continuity conditions of the displacement and the resultant force across Γ_1. By a similar way to the previous approach, one can find

$$\theta_{c1}(z) = U_{21}\theta_{b1}(z) \quad z \ge R \tag{18}$$

$$\theta_2(z) = V_{12}\overline{\theta_{b1}}\left(\frac{R^2}{z}\right) \quad z \le R \tag{19}$$

Obviously, this result cannot satisfy the continuity conditions at the interface Γ_2

Step 4: Repetition of steps 2 and 3

The method of analytical continuation is repeatedly performed across the two interfaces to achieve the additional terms $\theta_{an}(z)$, $\theta_{bn}(z)$, $\theta_{cn}(z)$, and $\theta_{n+1}(z)$, for $n = 2,3,4,\ldots$ then, by substitute above terms into Eq. (5) yields

$$\theta(z) = \begin{cases} U_{23}U_{12}\theta_0(z) + U_{23}V_{12}V_{32} \sum_{n=1}^{\infty} \theta_n\left(\frac{r^2}{\frac{R^2}{z}-\overline{z_A}}+z_A\right) & z \in S_3 \\ U_{12}\theta_0(z) + V_{12}V_{32} \sum_{n=1}^{\infty} \theta_n\left(\frac{r^2}{\frac{R^2}{z}-\overline{z_A}}+z_A\right) + V_{32}\sum_{n=1}^{\infty} \overline{\theta_n}\left(\frac{r^2}{z-z_A}+\overline{z_A}\right) & z \in S_2 \\ \theta_0(z) + V_{21}\overline{\theta_0}\left(\frac{R^2}{z}\right) + U_{21}V_{32} \sum_{n=1}^{\infty} \overline{\theta_n}\left(\frac{r^2}{z-z_A}+\overline{z_A}\right) & z \in S_1 \end{cases}$$

(20)

where the recurrence formulae for $\theta_n(z)$ is

$$\theta_n(z) = \begin{cases} U_{12}\theta_0(z) & n = 1 \\ V_{12}V_{32}\theta_{n-1}\left(\frac{r^2}{\frac{R^2}{z}-z_A}+\overline{z_A}\right) & n = 2,3,4,\ldots \end{cases}$$

(21)

$$\theta_0(z) = \frac{\mu_1 b_0}{2\pi i}\log(z-z_t)$$

3.2 Screw dislocation in core inclusion

Second, we consider a screw dislocation located in a core inclusion. Using the same procedure as Section 3.1, the solution of the other case in which the screw dislocation is located in region S_3 as follows

$$\theta(z) = \begin{cases} \theta_0(z) + V_{23}\overline{\theta_0*}\left(\frac{r^2}{z}\right) + U_{23}V_{12} \sum_{n=1}^{\infty} \overline{\theta_n}\left(\frac{R^2}{z-z_A}+\overline{z_A}\right) & z \in S_3 \\ \frac{\mu_2 b_0}{2\pi i}\log z + U_{32}\theta_0*(z) + V_{32}V_{12} \sum_{n=1}^{\infty} \theta_n\left(\frac{R^2}{\frac{r^2}{z}-\overline{z_A}}+z_A\right) & \\ \quad + V_{12} \sum_{n=1}^{\infty} \overline{\theta_n}\left(\frac{R^2}{z-z_A}+\overline{z_A}\right) & z \in S_2 \\ \frac{\mu_1 b_0}{2\pi i}\log z + U_{21}U_{32}\theta_0*(z) & \\ \quad + U_{21}V_{32}V_{12} \sum_{n=1}^{\infty} \theta_n\left(\frac{R^2}{\frac{r^2}{z}-\overline{z_A}}+z_A\right) & z \in S_1 \end{cases}$$

(22)

where the recurrence formulae for $\theta_n(z)$ is

$$\theta_n(z) = \begin{cases} U_{32}\theta_0*(z) & n = 1 \\ V_{32}V_{12}\theta_{n-1}\left(\frac{R^2}{\frac{r^2}{z}-z_A}+\overline{z_A}\right) & n = 2,3,4,\ldots \end{cases}$$

(23)

$$\theta_0(z) = \frac{\mu_3 b_0}{2\pi i}\log(z-z_t) \quad \theta_0*(z) = \frac{\mu_3 b_0}{2\pi i}\log\left(1-\frac{z_t}{z}\right)$$

4   Crack

The singular integral equations for this problem can easily be written down by using the screw dislocation solutions as the Green's function together with the principle of superposition.

First, to model the crack embedded in the infinite matrix or in core inclusion it is necessary to place a dislocation distribution $b_0(s)$ along the prospective site of the crack. In this case, we simply substitute b_0 by $b_0(s)$ and make integration along the crack. The corresponding homogeneous solution associated with a single crack can be expressed as

$$\theta_0(z) = \frac{\mu_1}{2\pi i} \int_L b_0(s) \log(z - z_t) \, ds \tag{24}$$

for crack in infinite matrix,

$$\theta_0 * (z) = \frac{\mu_3}{2\pi i} \int_L b_0(s) \log\left(1 - \frac{z_t}{z}\right) ds \tag{25}$$

for crack in core inclusion,

where $b_0(s)$ indicate the density function and z_t is a point on the crack.

Next, the principle of superposition can be applied due to the traction-free condition along the crack surface. It means, the total resultant force across the crack surface must be balance by the given resultant force across the crack segment in the unflawed media, i.e.

$$p(z) = -p^\infty(z) \tag{26}$$

The resultant force applied on the crack surface will be obtained by substituting Eqs. (24) and (20) $z \in S_1$ into Eq. (1) for crack located in infinite matrix and by substituting Eqs. (25) and (22) $z \in S_3$ into Eq. (1) for crack located in core inclusion.

On the other hand, the resultant force corresponding to the unflawed media can be obtained by substituting Eqs. (3) and (20) $z \in S_1$ into Eq. (1) for crack located in infinite matrix and by substituting Eqs. (3) and (20) $z \in S_3$ into Eq. (1) for crack located in core inclusion.

In addition, the single-valued condition of the dislocation density must be satisfied, i.e.

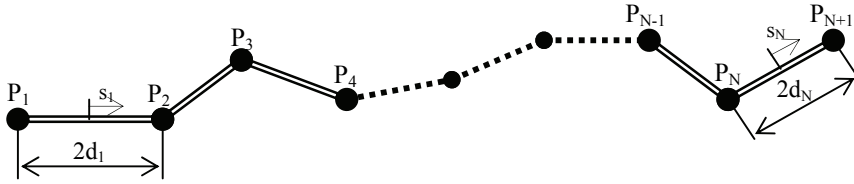$$\int_L b_0(s) ds = 0 \tag{27}$$

Figure 3: Division and nodal distribution of a crack.

Eq. (26) together with the subsidiary condition Eq. (27) will be solved numerically. In order to perform the numerical calculation, the crack is approximated by N line segments as indicated in Fig. 3. Since the dislocation distribution $b_0(s)$ preserves a square-root singularity at the vicinity of the crack tip, the interpolation formulae in local coordinates s_j *(1 ≤ j ≤ N)* are defined as

$$b_0(s_1) = b_{0,1} \left(\sqrt{\frac{2d_1}{d_1 + s_1}} - 1 \right) + b_{0,2} \tag{28}$$

for the left tip

$$b_0(s_N) = b_{0,N+1} \left(\sqrt{\frac{2d_N}{d_N - s_N}} - 1 \right) + b_{0,N} \tag{29}$$

for the right tip

$$b_0(s_j) = b_{0,j} \frac{d_j - s_j}{2d_j} + b_{0,j+1} \frac{d_j + s_j}{2d_j} \tag{30}$$

for intermediate segments

where d$_j$ *(1 ≤ j ≤ N)* are the half length of each line segment and $b_{0,j}$ *(1 ≤ j ≤ N+1)* are the unknown coefficients which can be determined numerically. Once the coefficients$b_{0,j}$ are solved, the mode-III stress intensity factors can be obtained accordingly as

$$K_{III}(tip-A) = -\sqrt{\pi} \lim_{s_1 \to 0} b_0(s_1) s_1^{1/2} = -\sqrt{\pi d_1} b_{0,1} \tag{31}$$

$$K_{III}(tip-B) = \sqrt{\pi} \lim_{s_{N+1} \to 2d} b_0(s_{N+1}) s_{N+1}^{1/2} = \sqrt{\pi d_N} b_{0,N+1} \tag{32}$$

5 Results and discussion

The main goal of this paper is to investigate the interaction between a crack and an eccentrically coated circular inclusion. This can be achieved by the determination of the stress intensity factors based on linear fracture mechanics.

5.1 Crack in infinite matrix

The results of normalized mode-III stress intensity factor versus the distance h/R for a crack in an infinite matrix with different μ_3/μ_1 are displayed in Fig. 4. In this example, $\mu_2/\mu_1 = 0.7$, r/R = 0.8, x_2/R = 0.9 are used. When $\mu_3/\mu_1 < 1$, the core inclusion is softer than the matrix, the stress intensity factors at tip-A increase as a crack approaches the inclusion. When $\mu_3/\mu_1 = 2$, the core inclusion is stiffer than the infinite matrix, it is interesting to see that the stress intensity factors at tip-A would not monotonically increase as a crack approaches the inclusion. Contradictorily, the K_{III} value increases as a crack is apart from the inclusion. This phenomena is more obvious when the core inclusion material is made more stiff than the matrix ($\mu_3/\mu_1 = 3$). Fig. 5 shows the variation of normalized mode-III stress intensity factor at tip-A versus the distance h/R with different μ_3/μ_1. In this example, $\mu_2/\mu_1 = 2$, r/R = 0.8, x_2/R = 0.9 are used. When the core inclusion is made stiffer than the matrix, the stress intensity factors at tip-A decrease as a crack approaches the inclusion. On the other hand, when the core inclusion is made softer than the matrix, it is interesting to see that the stress intensity factors at tip-A would not monotonically decrease as a crack approaches the inclusion. The results of normalized mode-III stress intensity factors versus the distance h/R for different thickness of coating layer are shown in Figs. 6-7. It is shown from Fig. 6 with $\mu_2/\mu_1 = 0.5$ and $\mu_3/\mu_1 = 2$, when the thickness of the coating layer is relatively large (r/R = 0.5), the core inclusion has less effect on the stress intensity factors, and the softer coating layer always gives enhancement effect on crack propagation. Similar observation can also applied to the case with $\mu_2/\mu_1 = 2$ and $\mu_3/\mu_1 = 0.7$ except that the stiffer coating layer always gives retardation effect on crack propagation as shown in Fig. 7. From the above results, we conclude that the larger thickness of coating layer would make the core inclusion less contribution on the stress intensity factor, and the results would tend to those corresponding to a two-phase composite. The results of normalized mode-III stress intensity factor versus the distance h/R with $\mu_2/\mu_1 = 0.5$ and $\mu_3/\mu_1 = 2$ are displayed in Fig. 8. It is interesting to see that the presence of core inclusion makes more contribution on the stress intensity factor as compared to the presence of the coating layer when the two circles are nearly in contact with each other (x_2/R = 0.999). Similar observation can also applied to the case with $\mu_2/\mu_1 = 2$ and $\mu_3/\mu_1 = 0.7$ as shown in Fig. 9. Note that the normalized mode-III stress intensity factors based on the present proposed method agree very
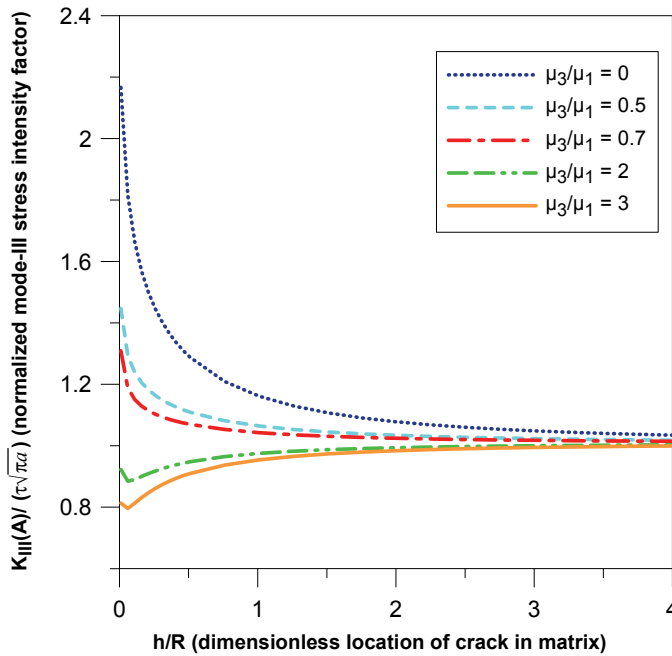
Figure 4: Normalized mode-III stress intensity factor versus dimensionless location of crack in matrix with different μ_3/μ_1 for $\mu_2/\mu_1 = 0.7$, r/R = 0.8, $x_2/R = 0.9$
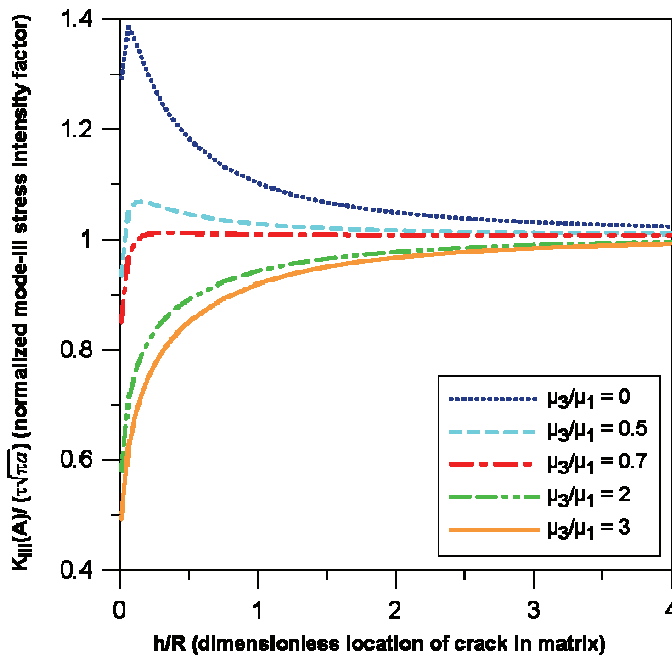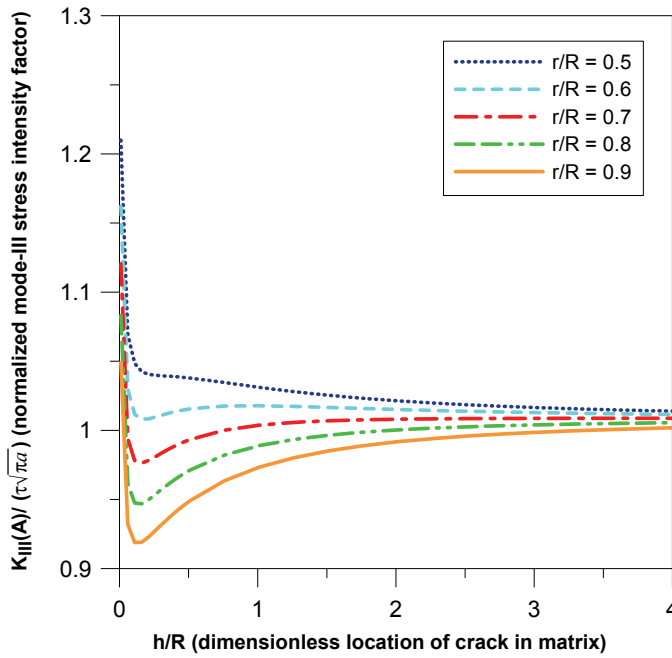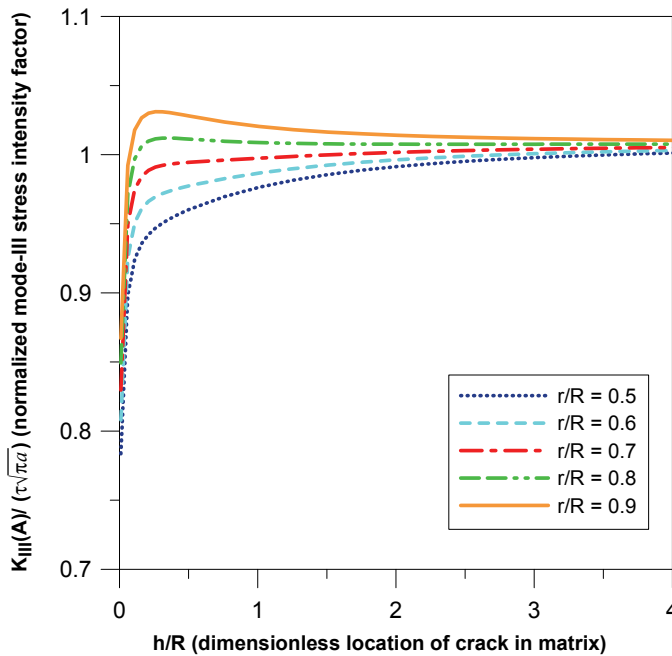

Figure 5: Normalized mode-III stress intensity factor versus dimensionless location of crack in matrix with different μ_3/μ_1 for $\mu_2/\mu_1 = 2$, r/R = 0.8, $x_2/R = 0.9$

Figure 6: Normalized mode-III stress intensity factor versus dimensionless location of crack in matrix with different r/R for $\mu_2/\mu_1 = 0.5$, $\mu_3/\mu_1 = 2$, $x_2/R = 0.9$

Figure 7: Normalized mode-III stress intensity factor versus dimensionless location of crack in matrix with different r/R for $\mu_2/\mu_1 = 2$, $\mu_3/\mu_1 = 0.7$, $x_2/R = 0.9$
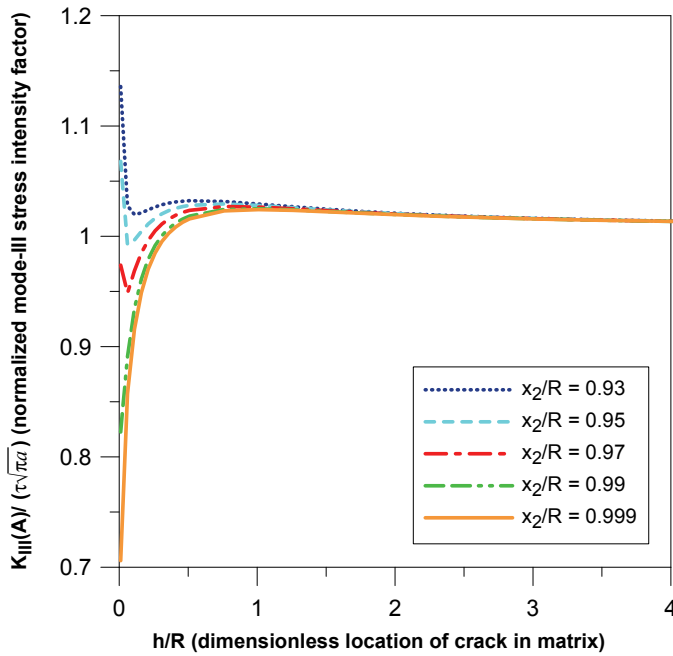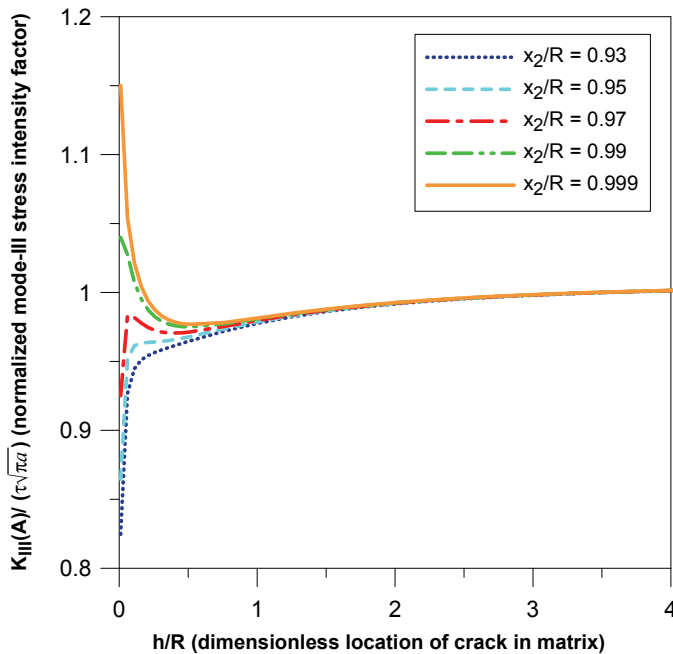
Figure 8: Normalized mode-III stress intensity factor versus dimensionless location of crack in matrix with different x_2/R for $\mu_2/\mu_1 = 0.5$, $\mu_3/\mu_1 = 2$, $r/R = 0.5$

Figure 9: Normalized mode-III stress intensity factor versus dimensionless location of crack in matrix with different x_2/R for $\mu_2/\mu_1 = 2$, $\mu_3/\mu_1 = 0.7$, $r/R = 0.5$
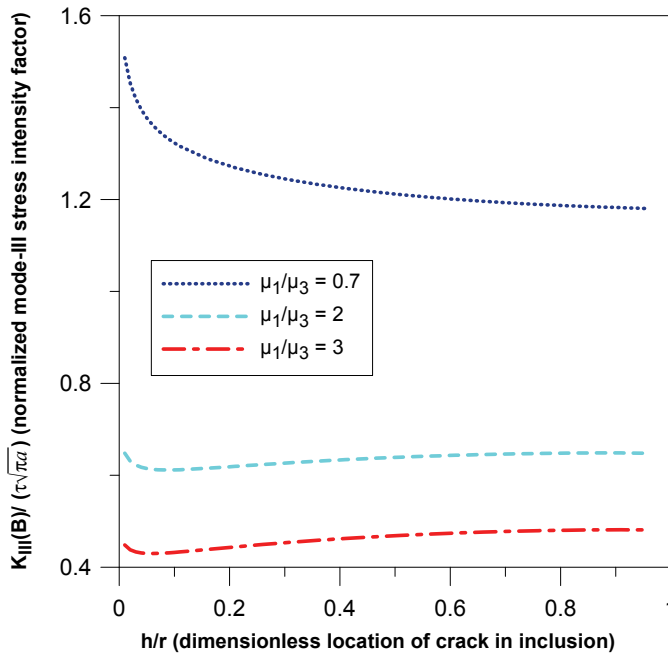
Figure 10: Normalized mode-III stress intensity factor versus dimensionless location of crack in inclusion with different μ_1/μ_3 for $\mu_2/\mu_3 = 0.7$, $r/R = 0.8$, $x_2/R = 0.9$

well with the exact results if the number of line segment is chosen as $N = 30$. It is also worthy to note that all stress intensity factors presented here are obtained by summation of series solution up to the first five terms, since they are checked to achieve a good approximation for most combination materials. Table 1 shows that the contributions of the stress intensity factors for leading terms of the series when $\mu_2/\mu_1 = 2$, $\mu_3/\mu_1 = 0.1$, $r/R = 0.9$. It is likely to see that the leading five terms make over 99% contribution, making the series solution rapidly convergent. This demonstrates the accuracy and the efficiency of the proposed method.

5.2 Crack in core inclusion

The results of normalized mode-III stress intensity factor at tip-B versus the distance h/R for a crack in a core inclusion with different μ_1/μ_3 are shown in Fig. 10. In this example, $\mu_2/\mu_3 = 0.7$, $r/R = 0.8$, $x_2/R = 0.9$ are used. It is seen that, when $\mu_1/\mu_3 = 0.7$, the stress intensity factors at tip-B increase as a crack approaches the coating layer. However, when the core inclusion is softer than the matrix, it is interesting to see that the stress intensity factors at tip-B would not monotonically

Table 1: Contribution of the leading terms n = 1-5 for mode-III stress intensity factors

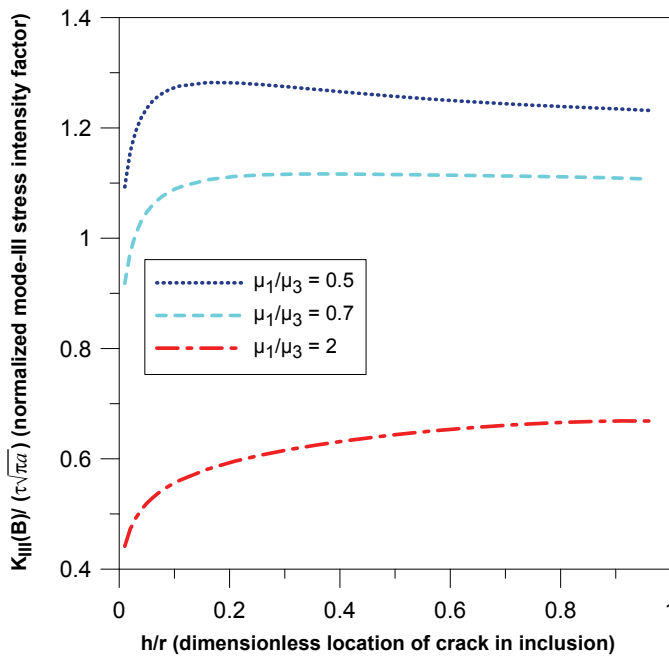| Terms	K3	Contribution (%)
1	1.069659	75.61351835
2	1.100616	18.44626964
3	1.108168	4.496935078
4	1.110009	1.09653679
5	1.110458	0.267472665

Figure 11: Normalized mode-III stress intensity factor versus dimensionless location of crack in inclusion with different μ_1/μ_3 for $\mu_2/\mu_3 = 2$, $r/R = 0.8$, $x_2/R = 0.9$

increase as a crack approaches the coating layer. On the other hand, when both the matrix and coating layer are made stiffer than the core inclusion, the stress intensity factors at tip-B monotonically decrease as a crack approaches the coating layer as shown in Fig. 11. The results of normalized mode-III stress intensity factor at tip-B versus the distance h/R for different thickness of coating layer are shown in Figs. 12-13. It is shown from Fig. 12, when the thickness of the coating layer is
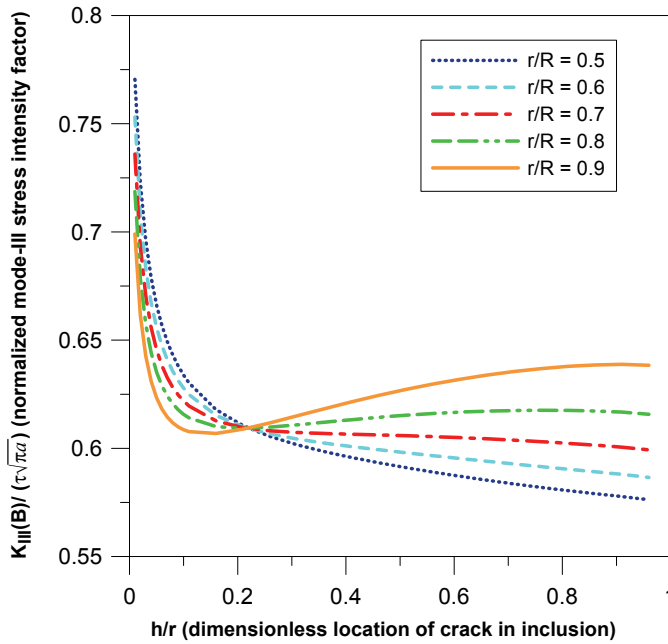
Figure 12: Normalized mode-III stress intensity factor versus dimensionless location of crack in inclusion with different r/R for $\mu_2/\mu_3 = 0.5$, $\mu_1/\mu_3 = 2$, $x_2/R = 0.9$
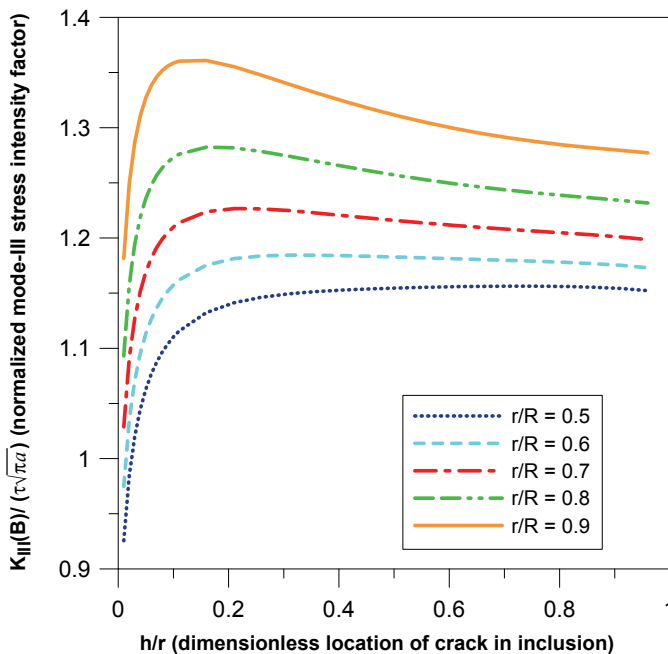

Figure 13: Normalized mode-III stress intensity factor versus dimensionless location of crack in inclusion with different r/R for $\mu_2/\mu_3 = 2$, $\mu_1/\mu_3 = 0.5$, $x_2/R = 0.9$
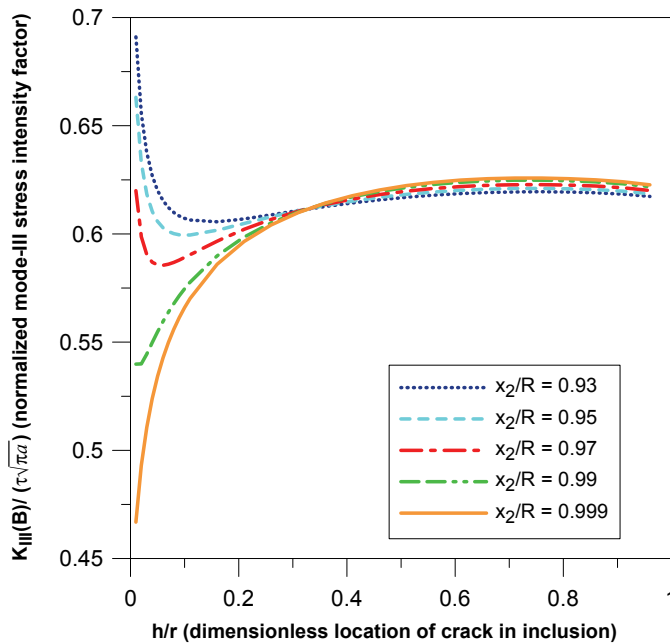
Figure 14: Normalized mode-III stress intensity factor versus dimensionless location of crack in inclusion with different x_2/R for $\mu_2/\mu_3 = 0.5$, $\mu_1/\mu_3 = 2$, $r/R = 0.8$
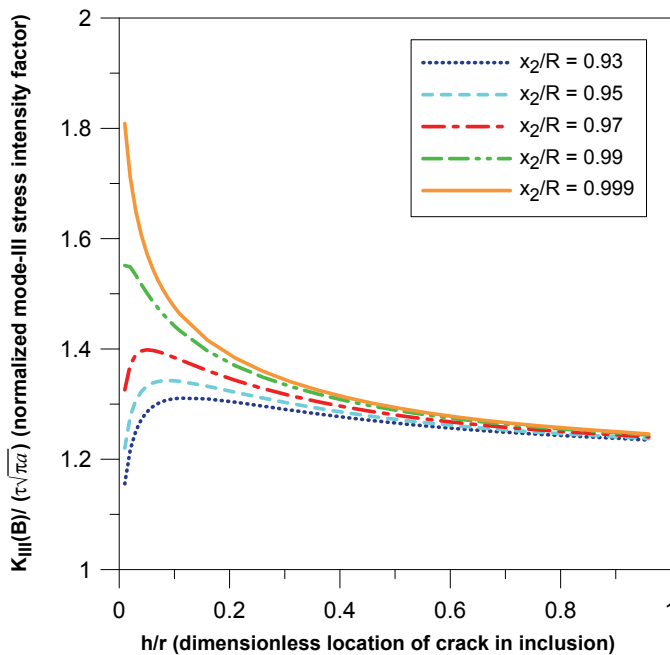

Figure 15: Normalized mode-III stress intensity factor versus dimensionless location of crack in inclusion with different x_2/R for $\mu_2/\mu_3 = 2$, $\mu_1/\mu_3 = 0.5$, $r/R = 0.8$

large enough (r/R = 0.5), the presence of matrix has less effect on the stress intensity factors, and the softer coating layer always gives enhancement effect on crack propagation. Similarly, when the thickness of the coating layer is large enough (r/R = 0.5), the presence of matrix has no significant effect on the stress intensity factor, and the stiffer coating layer will always gives retardation effect on crack propagation as shown in Fig. 13. When the two circles are nearly in contact with each other (x_2/R = 0.999), the normalized mode-III stress intensity factors at tip-B monotonically decrease (or increase) with decreasing of the distance h/R if the core inclusion is softer (or stiffer) than the matrix as shown in Fig. 14 and Fig. 15. We can conclude that, when the two circles are nearly in contact with each other (x_2/R = 0.999), the presence of core inclusion plays more contribution on stress intensity factors than the presence of coating layer.

6   Conclusions

Antiplane interaction between a single crack with a non-uniformly coated circular inclusion under a remote uniform shear load is presented in this paper. By applying the existing complex potential solutions for a screw dislocation function, the logarithmic singular integral equations for a line crack in infinite matrix and core inclusion are formulated. Numerical calculations are performed to investigate the effect of material properties and geometric configurations on mode-III stress intensity factors. The results presented in this work would be helpful for engineers to prevent unstable crack propagation occurring in a three-phase composite with an eccentric circular inclusion.

References

Atkinson, C. (1972): The interaction between a crack and an inclusion. *International Journal of Engineering Science*, vol. 10, pp. 127-136.

Chao, C. K.; Lee, J. Y. (1996): Interaction between a crack and a circular elastic inclusion under remote uniform heat flow. *International Journal of Solids and Structures*, vol. 33, pp. 3865-3880.

Chao, C. K.; Shen, M. H. (1995): Solutions of thermoelastic crack problems in bonded dissimilar media or half-plane medium. *International Journal of Solids and Structures*, vol. 32, pp. 3537-3554.

Chen, F. M. (2011): Edge dislocation interacting with a nonuniformly coated circular inclusion. *Archieve of Applied Mechanics*, vol. 80, no. 8, pp. 1117-1128.

Chen, Y. Z.; Chen, R. S. (1997): Interaction between curved crack and elastic inclusion in an infinite plate. *Archive of Applied Mechanics*, vol. 67, pp. 566-575.

Chen, Y. Z.; Cheung, Y. K. (1990): New integral equation approach for the crack problem in elastic half-plane. *International Journal of Fracture*, vol. 46, pp. 57-69.

Erdogan, F.; Gupta, G. (1975): The inclusion problem with a crack crossing the boundary. *International Journal of Fracture*, vol. 11, pp. 13-27.

Erdogan, F.; Gupta, G. D.; Ratwani, M. (1974): Interaction between a circular inclusion and an arbitrarily oriented crack. *Journal of Applied Mechanics*, vol. 41, pp. 1007-1013.

Shen, M. H.; Chen, S.N.; Chen, F, M. (2006): A piezoelectric screw dislocation interacting with a nonuniformly coated circular inclusion. *International Journal of Engineering Science*, vol. 40, pp. 1-13.

Wang, X.; Zhong, Z. (2003): A circular inclusion with a nonuniform interphase layer in anti-plane shear. *International Journal of Solids and Structures*, vol. 40, pp. 881-897.